THE JOURNAL OF
PHYSICAL CHEMISTRY C

Article

pubs.acs.org/JPCC

Tracking the Effect of Sodium Insertion/Extraction in Amorphous and Anatase TiO_2 Nanotubes

Jun Li,[†,∥] Jian Liu,[⊥,§,∥] Qian Sun,[§] Mohammad Norouzi Banis,[‡] Xueliang Sun,[*,§] and Tsun-Kong Sham[*,†,‡]

[†]Department of Chemistry and [‡]Soochow University-Western University Centre for Synchrotron Radiation Research, University of Western Ontario, 1151 Richmond Street, London, Ontario N6A 5B7, Canada

[§]Department of Mechanical and Material Engineering, University of Western Ontario, London, Ontario N6A 5B9, Canada

Supporting Information

ABSTRACT: We report a mechanistic investigation of the electrochemical behavior of TiO_2 nanotubes (NTs) in amorphous and anatase phases during sodiation/desodiation. The local structure variations of these two host structures upon Na^+ uptake/release are comparatively examined by X-ray absorption near edge structure (XANES) at the Ti K and L, O K, and Na K edges. Upon Na^+ insertion/extraction, the surface/near surface XANES analysis at the Ti K edge suggests that the surface/near surface of TiO_2 NTs in both phases is partially reduced to metallic Ti from the unstable sodium titanate formed at the electrolyte/electrode interface, and the sodiation of amorphous NTs is more effective than anatase ones. More importantly, it further reveals that irreversible phase transformations from pure amorphous and anatase TiO_2 to amorphous sodium titanate take place on the NT surface/near surface after the first cycle of discharge/charge. The bulk XANES analysis at the Ti L edge demonstrates that irreversible phase transformation also proceeds in the bulk of these two phase structures, where, however, the formation stable amorphous sodium titanate is observed. All the findings are corroborated by energy dispersive X-ray (EDX) spectroscopy, X-ray diffraction (XRD), and XANES analysis at the O K and Na K edges.

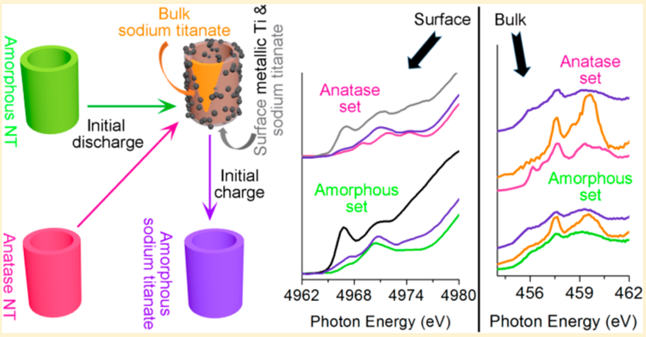

■ INTRODUCTION

Current research in TiO_2 engineering has made a promising progress toward its applications in photocatalysis,[1,2] dye-sensitized solar cells,[3,4] supercapacitors,[5,6] and rechargeable battery systems such as lithium-ion batteries (LIBs) and sodium-ion batteries (SIBs).[7−10] As for the latter, TiO_2 has been shown to exhibit excellent cyclability and high rate capability as an anode material in LIBs and SIBs, due to its open structure for the fast transport of lithium and sodium ions.[7,8] Nonetheless, although both alkali metal ions have theoretically comparable activation barrier for insertion in/extraction out of titania lattice,[11] their ionic size difference has resulted in different electrochemical reaction mechanisms. For example, the reaction of Li^+ with anatase TiO_2 exhibits a two-phase transition process, showing reversible plateaus in the potential−capacity curve,[7,12,13] whereas the reaction of Na^+ with anatase TiO_2 shows no plateau, which has usually been assigned to its pseudocapacitive nature (i.e., Na^+ rather adsorbs than diffuses inside the lattice) during cycling.[8,14] As a thorough understanding of the lithiation process in nanostructured TiO_2 anodes has been worked out in a previous report,[7] efforts in this work deal with the sodiation mechanism in nanostructured TiO_2 anodes.

Since the initial work of Xiong et al.,[15] the use of TiO_2 as a host for Na^+ accommodation has been widely studied. Recent development of efficient TiO_2 nanomaterials for Na^+ insertion concentrates on their phase differences; particularly the focus is placed on amorphous[15,16] and anatase TiO_2[17−20] due to their excellent cyclability and high rate performance. First, the highly distorted (locally) amorphous structure with rich defects and voids is desirable for the accommodation of Na^+. Also, compared to crystalline TiO_2, the diffusion of Na^+ can be enhanced in amorphous TiO_2 which provides more percolation pathways due to its increased interfacial regions.[15] Second, anatase TiO_2 also shows its excellent capacity for Na^+ accommodation due to the following considerations: (1) the two-dimensional Na^+ diffusion tunnels along the *a* and *b* axes with a size of 3.725 Å × 3.785 Å (Figure S1 in Supporting Information) suitable for the interstitial accommodation of Na^+ (1.02 Å), (2) low insertion potential (∼1 V vs Na^+/Na), and (3) high theoretical capacity of ∼335 mAh g^{-1}.[8,18,19,21−23]

However, the Na^+ reaction mechanism with TiO_2 is still not clearly understood although many efforts have been made. For example, Xiong et al.[15] and Kim et al.[9] applied XANES analysis on the progress of Na^+ insertion/extraction in amorphous and anatase TiO_2, and both provide evidence for the reversible Na^+

Received: February 3, 2017
Revised: April 14, 2017
Published: April 25, 2017

DOI: 10.1021/acs.jpcc.7b01106
J. Phys. Chem. C 2017, 121, 11773−11782

uptake/release with charge neutrality considerations, i.e., that the reduction of Ti^{4+} to Ti^{3+} occurs upon Na^+ insertion and the oxidation of Ti^{3+} to Ti^{4+} takes place upon Na^+ extraction. Similarly, additional ex situ X-ray diffraction (XRD), nuclear magnetic resonance (NMR), and electrochemical studies further corroborate the reversible Na^+ insertion/extraction without affecting the integrity of the TiO_2 host structure.[14,16,24,25] Nevertheless, a recent finding by Wu et al.[8] showed an irreversible TiO_2 phase transformation from anatase to a stable amorphous sodium titanate along with the formation of metallic Ti upon the initial sodiation of anatase TiO_2 nanoparticles. They claimed that the newly formed sodium titanate structure is in the amorphous form instead of the initially crystalline anatase TiO_2; this accounts for the reversible Na^+ uptake/release as well as the superior SIB performance. Accordingly, strong evidence is provided by in situ XRD, ex situ X-ray photoelectron spectroscopy (XPS), and Raman spectroscopy. Yet, the structure of as-detected sodium titanate remains unknown, and the evidence for irreversible phase transformation, especially the formation of metallic Ti, has only been demonstrated from surface characterization (i.e., XPS) whereas the sodiation mechanism in the bulk of TiO_2 is still lacking. Therefore, despite the excellent SIB performance reported in literature using TiO_2,[19,21,25] a further study to glean a comprehensive understanding of the Na^+ insertion/extraction mechanism in TiO_2 is of foremost importance, in order to achieve the desired energy and power densities of SIB using TiO_2 as an anode material.

In this paper, we report an experiment in which anodic TiO_2 NT attached on Ti metal foil is used directly as the anode material in a SIB system for the study of Na^+ accommodation due to its unique structure and alignment, allowing for efficient ionic/electronic mobility.[21] XANES, arguably the most suitable technique to investigate the local structure variation of TiO_2 upon sodiation/desodiation, is used. As XANES records the core level excitation of element of interest, the effect of Na^+ insertion/extraction on the local structure of TiO_2 can be tracked from site specific perspectives, i.e., Ti, O, and Na. Moreover, XANES is a local probe; it has a unique advantage for studying amorphous structures. In addition, these elements of interest have their core levels in the soft X-ray region, and XANES recorded in total electron yield (TEY) and partial fluorescence yield (PLY), respectively, can be employed to track the surface/near surface and bulk local structures due to their different probing depths.[26,27] Herein, we provide an insight of the mechanism for Na^+ reaction with TiO_2 NTs, in which we track the progress of Na^+ uptake/release in amorphous and anatase structures with depth information by comparatively examining the XANES at the Ti K-edge, Ti $L_{3,2}$-edge, O K-edge, and Na K-edge with TEY and PFY.

■ EXPERIMENTAL SECTION

Materials and Methods. Vertically aligned TiO_2 NTs were prepared by an electrochemical anodization method. In a standard two-electrode electrochemical cell, Ti foil (0.1 mm thick, Goodfellow) with a size of 1 cm × 0.5 cm was the anode while a Pt wire was used as cathode. The electrolyte composition included 0.3 wt % NH_4F (ACS, 98.0% min, Alfa Aesar), 2 vol % H_2O, and ethylene glycol. To obtain ordered NTs with good geometry and alignment, a two-step anodization procedure was applied. In the first step, Ti foil was anodized at 50 V for 4 h, and then the first TiO_2 layer was removed by ultrasonication in 1 M HCl. Next, the refreshed Ti foil was rinsed with water and then ethanol several times and then dried with N_2 gas. In the second step, to ensure the conductivity of Ti substrate for the following battery test, one side of Ti foil was covered by nail polish to prevent Ti from oxidization. For the second anodization, the same procedure as in the first step was employed, and the one side of refreshed Ti foil was anodized at 50 V for 40 min. Later on, the as-grown NTs attached to the Ti substrate were rinsed with ethanol several times to remove the excess electrolyte and dried with N_2 gas, and the nail polish on the back side was carefully removed by ethanol infiltrated Kimwipes. To initiate the anatase crystallization, the as-grown amorphous NTs were annealed at 450 °C for 2 h to obtain anatase TiO_2 NTs.[26]

Electrochemical Characterization. The electrochemical performance of amorphous and anatase TiO_2 NTs on Ti substrates (5 mm × 5 mm) was evaluated in coin-type half cells. The coin-type half cells were assembled in an argon-filled glovebox ($[O_2] < 1$ ppm, $[H_2O] < 1$ ppm), using polypropylene (Celgard 3501) as the separator and Na metal as the counter electrode. The electrolyte was 1 M $NaClO_4$ in ethylene carbonate (EC) and propylene carbonate (PC) in a volume ratio of 1:1. Charge−discharge cycling at a constant current mode was carried out on the Arbin BT-2000 battery test system. The electrochemical performance was measured in a voltage range of 0.01−2.0 V at room temperature. The specific areal capacity (μAh cm^{-2}) was used to compare the performance of amorphous and anatase TiO_2 NTs because it is unable to measure the accurate amount of TiO_2 NTs on the Ti substrates. TiO_2 NTs charged or discharged at certain potentials were harvested by disassembling the coin-type half cells in the glovebox and washed with the PC solvent. Then the TiO_2 NTs samples were sealed with Kapton tapes and put into an argon-filled container to prevent exposure to the air before synchrotron measurements.

Morphology and Structural Characterizations. Scanning electron microscopy (SEM) images and energy dispersive X-ray (EDX) mapping were recorded by a LEO (Zeiss) 1540 XB SEM facility operating at 10 kV. XANES measurements were performed at the Canadian Light Source (CLS, Saskatoon, SK, Canada). The Ti K-edge was recorded at the Soft X-ray Microcharacterization Beamline (SXRMB) using Si(111) monochromator crystals,[28] whereas the Ti $L_{3,2}$-edge, O K-edge, and Na K-edge were tracked at the Spherical Grating Monochromator (SGM) beamline.[29] Note that both beamlines have an energy resolution $E/\Delta E > 5000$, and XANES experiments were measured using total electron yield (TEY) and partial fluorescence yield (PFY). Typically, TEY and PFY at shallow absorption edges (soft X-rays region) provide different probing depths which can be used as surface/near surface- and bulk-sensitive techniques, respectively. Whereas TEY tracks the outgoing secondary electrons by measuring the specimen current, PFY collects the outgoing characteristic X-ray fluorescence of the element of interest using four silicon drift detectors.[26,30] To erase the X-ray polarization effect, a glancing angle of 45° was applied to all the X-ray measurements where the vertically aligned NTs attached on Ti substrate were mounted on a Cu holder and facing up. Whereas TEY was recorded by monitoring the specimen current, PFY was collect with a detection angle of 90° to the incident X-ray beam.[27] All spectra were normalized to the incident photon flux.

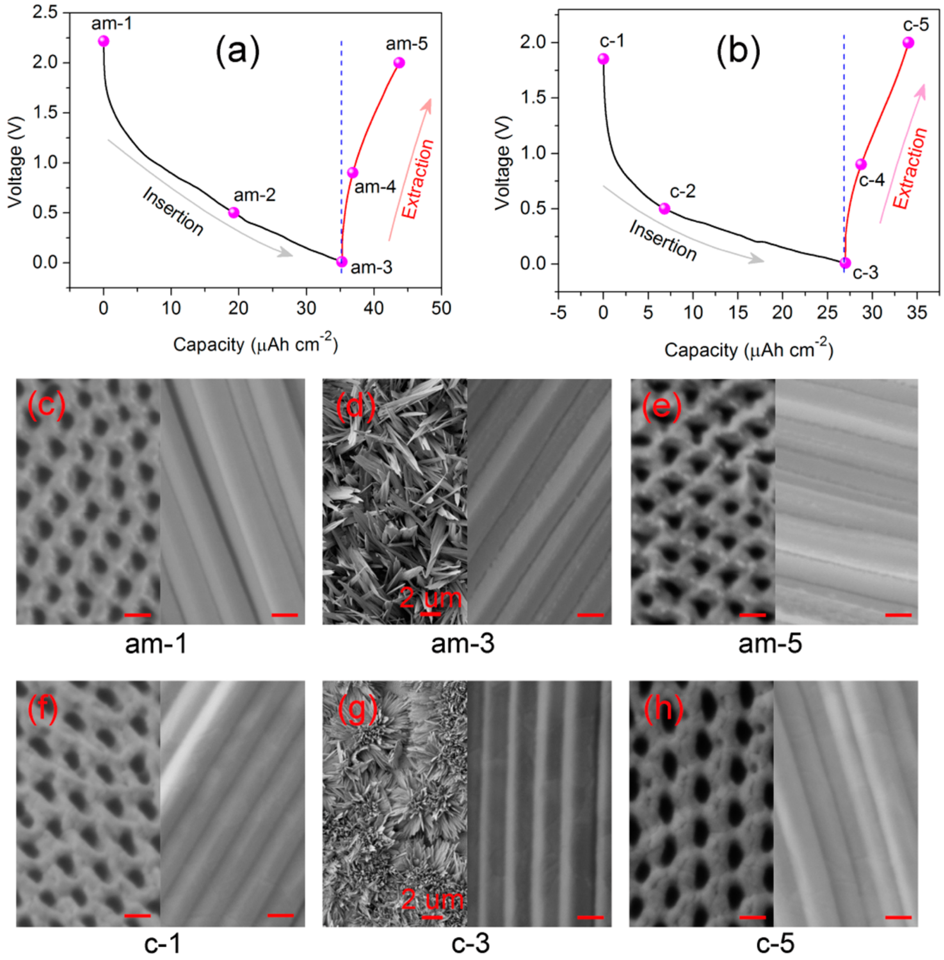

Figure 1. First-cycle discharge/charge curves of (a) amorphous and (b) crystalline TiO_2 NTs with potential plotted as a function of areal capacity (μAh cm^{-2}). Five discharge/charge potentials are labeled where the following characterization and analysis are carried out. (c−e) Top/side SEM views of am-1, am-3, and am-5 NT specimens as indicated in (a). (f−h) Top/side SEM views of c-1, c-3, and c-5 NT specimens as indicated in (b). The unlabeled scale bars of SEM images are 100 nm.

■ RESULTS AND DISCUSSION

Charge and Discharge Profile and Morphology. The initial discharge and charge profiles of amorphous and crystalline TiO_2 NTs are displayed in Figure 1a and Figure 1b, respectively. Consistent with earlier reports,[8,9,15] the shapes of sodium discharging/charging curves of both amorphous and crystalline TiO_2 do not show obvious potential plateaus. For the sake of convenience, the areal capacities are provided in this study as the two sets of NTs were synthesized from the same batch and the net mass of the active material was difficult to quantify (where the total mass of TiO_2 NT thin film and Ti substrate remains constant before and after crystallization, i.e., no mass change of active material during crystallization). As shown in Figure 1a and Figure 1b, the amorphous TiO_2 NTs generally delivers a higher areal capacity than the crystalline ones, further corroborated by the long-term cycling performance where both TiO_2 phase structures exhibit excellent cyclability upon Na^+ uptake/release (Figure S2). It is mainly due to the defect-rich and disordered structure of amorphous TiO_2, allowing the easier accommodation of sodium ions.[7,10,16]

In an attempt to gain insights into Na^+ insertion/extraction mechanism of TiO_2 NTs, we prepared a number of amorphous and crystalline NT specimens, discharged/charged respectively at five different potentials during the first cycle for further characterization and analysis. As highlighted in Figure 1a and Figure 1b, x-1 (where x is am or c) stands for the freshly as-made NT specimen, whereas x-2 and x-3 are discharged to 0.5 and 0.01 V, respectively, and x-4 and x-5 are individually charged back to 0.9 and 2.0 V, respectively.

To track the morphology evolution of NTs during the sodiation/desodiation process, we recorded the top and side SEM images of x-1, x-3, and x-5 as shown in Figure 1c−e and Figure 1f−h for amorphous and crystalline TiO_2 NT specimens, respectively. Apparently, both sets of TiO_2 NTs (with an inner NT diameter of ∼70 nm and a NT wall thickness of ∼30 nm) with a thickness of 4 μm (Figure S3) undergo a negligible morphology change upon Na^+ insertion/extraction. It suggests that the stress and strain in TiO_2 induced by Na^+ uptake/release can be easily accommodated by the nanotubular structure due to its large surface to volume ratio as well as the presence of voids.[7] To evaluate the sodium accommodation capacities of amorphous and crystalline TiO_2 NTs, we used energy dispersive X-ray (EDX) elemental analysis (Figure S4), which demonstrates the Na/Ti atomic ratios of 0 (am-1), 0.72 (am-2), 1.34 (am-3), 1.05 (am-4), and 0.85 (am-5) for amorphous TiO_2 NT specimens and 0 (c-1), 0.05 (c-2), 0.43 (c-3), 0.32 (c-4), and 0.22 (c-5) for crystalline ones. On the basis of the EDX results, three points should be noted. First, it is clear that amorphous TiO_2 NT has a much higher Na^+ accommodation capacity than the crystalline counterpart

DOI: 10.1021/acs.jpcc.7b01106
J. Phys. Chem. C 2017, 121, 11773−11782

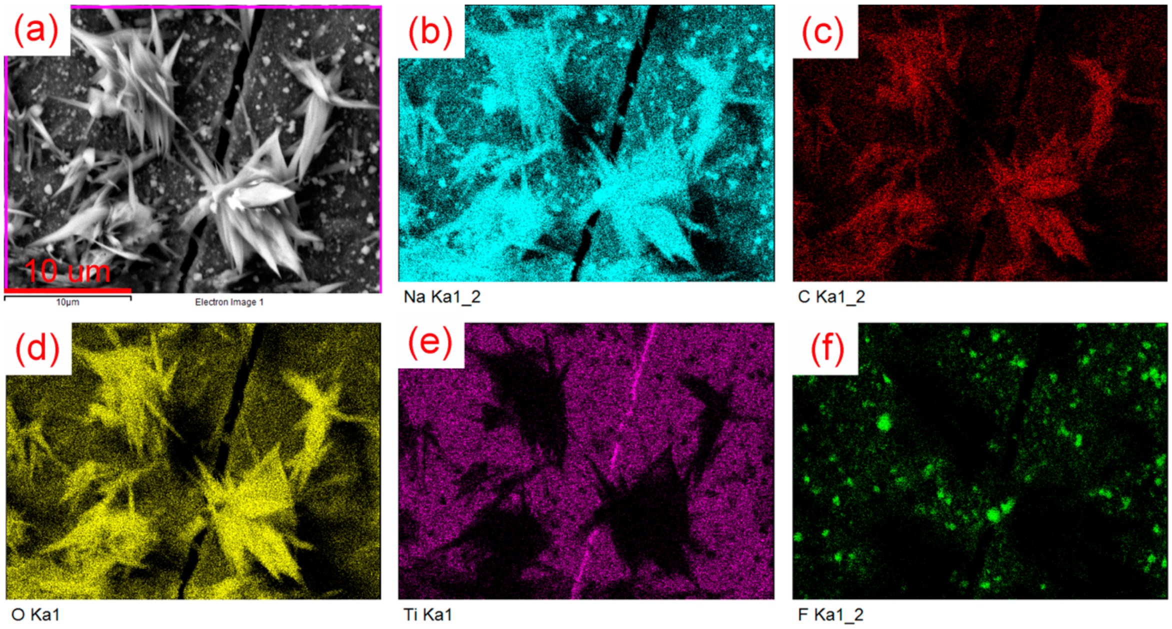

Figure 2. EDX mapping of am-2 NT specimen: (a) SEM image of the region of interest; (b−f) elemental mappings for Na (cyan), C (red), O (yellow), Ti (purple), and F (green), respectively.

due to the larger Na/Ti atomic ratio of the former, in good agreement with the electrochemical performance results (Figure 1a, Figure 1b, and Figure S2). Second, both am-5 and c-5 show the presence of sodium after being fully charged back to 2.0 V. It suggests that a certain amount of Na^+ is irreversibly trapped into the titania host structures (both phases) during the first cycle. Last, the Na/Ti atomic ratio difference between x-3 and x-5 indicates that nearly 0.49 and 0.21 Na per TiO_2 can be reversibly accommodated within the amorphous and crystalline TiO_2 NTs, respectively, doubly confirming that amorphous TiO_2 is a better host for Na^+ storage than the crystalline form.

It is noteworthy that flower-like structures show up and cover the top surface of NTs once discharged to 0.01 V (Figure 1d and Figure 1g), and they disappear when NTs are fully charged (Figure 1e and Figure 1h). To determine the chemical components involved in those flower-like structures, EDX mapping of amorphous NTs (am-2) is taken at a region (shown in Figure 2a) with less densification of those structures. As shown in Figure 2, Na, C, O, Ti, and F elements are included in this area, and the top flower-like structures are mainly composed of Na, C, and O. EDX mapping of crystalline NTs shows similar finding (Figure S5). The structural analysis of these flower-like structures will be addressed later.

Crystal Structure upon Na^+ Insertion and Extraction. The crystal structure and crystallinity evolution of TiO_2 NTs upon Na^+ insertion/extraction were tracked by X-ray diffraction (XRD). As shown in Figure S6, amorphous NT specimens, as expected, only exhibit the Ti metal reflections from the substrate. Figure 3a shows XRD results of crystalline TiO_2 NTs during Na^+ uptake/release. Beyond the dominant Ti substrate signals (JCPDS 44-1294, labeled with $*$), the presence of (101) and (200) reflections attributed to anatase TiO_2 (JCPDS 65-5714) is observed, of which the magnification of (101) reflection is displayed in Figure 3b for clarity. Upon discharge to 0.5 V (c-2), the anatase crystal structure as well as the crystallinity is retained, suggesting that the areal capacity observed at this point (Figure 1b) is mainly associated with a pseudocapacitive process (i.e., Na^+ is adsorbed rather than stored inside the lattice).[8,14] Once discharged to 0.01 V (c-3), the anatase host structure suffers a sharp crystallinity decrease, and the loss of crystallinity is not restored even when the NT specimen is fully charged (c-5).

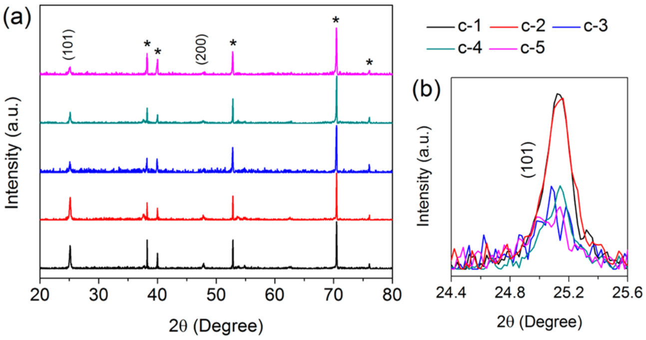

Figure 3. (a) XRD results of c-1, c-2, c-3, c-4, and c-5 NT specimens (indicated in Figure 1b). Peaks labeled with $*$ can be assigned to the Ti substrate. (b) Magnification of the 2θ region from 24.4° to 25.6°, showing the evolution of the (101) peak during Na^+ insertion/extraction.

Several interesting points can be noticed here. First of all, the decrease of anatase crystallinity from c-2 to c-3 indicates that an amorphization process results from the electrochemical reaction between anatase TiO_2 host and external Na^+. More importantly, no regain of the partially lost crystallinity in the charge process unambiguously illustrates that the amorphization process observed in the initial discharge process is irreversible. However, it is also apparent that a certain amount of anatase structure remains intact during the discharge/charge process, implying that Na^+ proceeds inhomogeneously in the anatase TiO_2 NT specimen upon electrochemical interaction. These findings are clearly in contrast to Kim et al.[9] and Gonzalez[14] et al. but rather in line with Wu et al.[8]

Tracking the Na^+ Insertion and Extraction from the Ti Perspective with XANES. To disclose the effect of Na^+

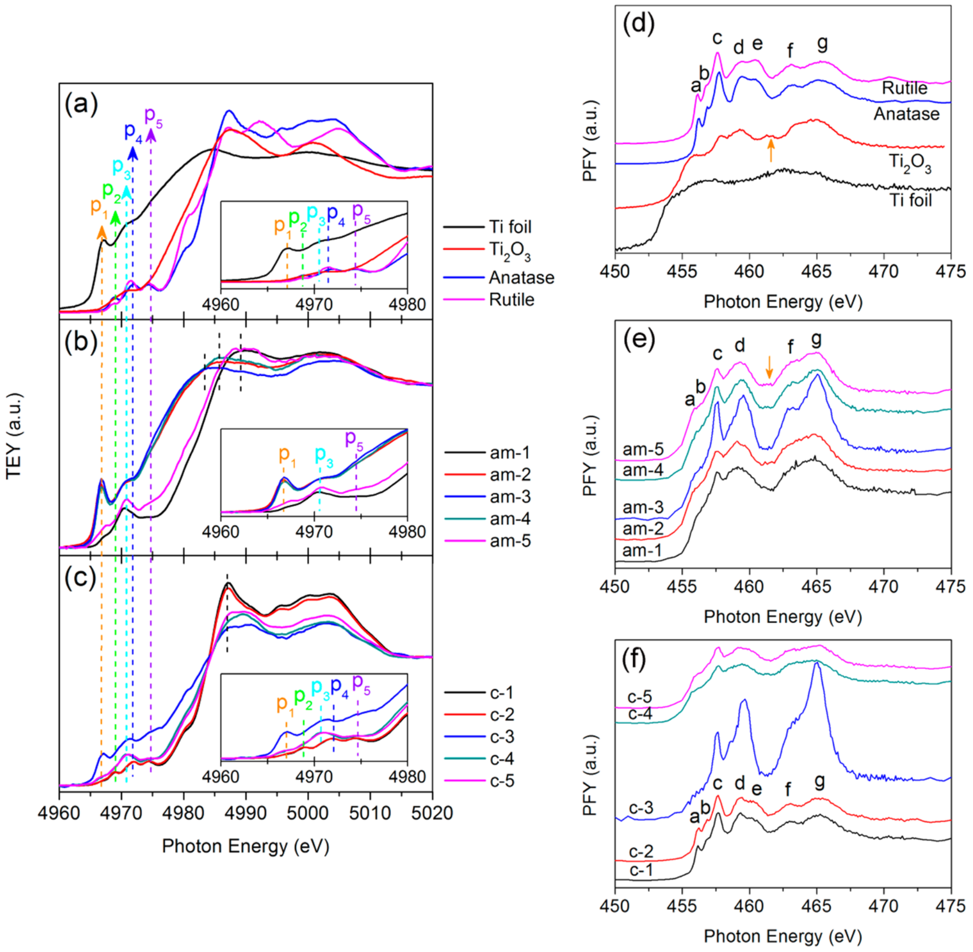

Figure 4. Ti K-edge TEY XANES spectra of (a) standards including Ti foil, Ti_2O_3, anatase and rutile TiO_2, (b) amorphous and (c) anatase NT specimens discharged/charged at five potentials during the first cycle shown in Figure 1a and Figure 1b. The insets show the magnified views of the corresponding pre-edge regions. Ti $L_{3,2}$-edge PFY XANES spectra of (d) standards including Ti foil, Ti_2O_3, anatase and rutile TiO_2, (e) amorphous and (f) anatase NT specimens discharged/charged at five potentials during the first cycle are indicated in Figure 1a and Figure 1b.

insertion/extraction on the electronic structures of amorphous and anatase TiO_2 NT hosts, Ti K-edge XANES recorded in total electron yield (TEY) and Ti L-edge XANES measured in partial fluorescence yield (PFY) are applied as surface/near surface and bulk analysis techniques, respectively. Note that TEY collects mainly the secondary electrons which have a shallow electron escape depth of several to tens of nanometers (surface/near surface-sensitive), whereas PFY compiles the X-ray fluorescence which has an energy-dependent X-ray attenuation length and can reach hundreds of nanometers specifically at the Ti L-edge (bulk-sensitive, Figure S7).[26,27]

Parts a−c of Figure 4 show the Ti K-edge TEY XANES spectra of amorphous and anatase NT specimens discharged/charged at different potentials (Figure 1a and Figure 1b) as well as standards (Ti foil, Ti_2O_3, anatase and rutile TiO_2) for comparison. In general, the interpretation of the Ti K-edge is intricate, of which the main-edge features (above 4980 eV) can be assigned to the dipole transition from Ti 1s to 4p states, whereas the pre-edge features (before 4980 eV) are usually ascribed to electronic transitions to hybridized states between Ti 4p and 3d orbitals based on a mixture of quadrupole and dipole excitations.[7,31−34] The pre-edge features can be used as fingerprints for tracking the local structure modification of Ti atoms. As shown in Figure 4a, both anatase and rutile standards deliver the similar pre-edge features. Whereas peak p_2 can be attributed to the quadrupole transition from Ti 1s to t_{2g} states of Ti absorber, feature p_4 originates from dipole transitions from Ti 1s to p states covalently hybridized with both t_{2g} states of Ti neighbor and e_g states of Ti absorber, and resonance p_5 can be assigned to dipole transition from Ti 1s to p states covalently hybridized with the e_g states of Ti neighbor.[7,31,35−37] As one extra electron is introduced in TiO_2, its occupancy in Ti 3d orbital interferes with the O ligands, resulting in the broad pre-edge feature, negative shift of the edge onset, and the lower intensity of main-edge features at the Ti K-edge of Ti_2O_3. For the case of Ti foil, although the origins of its broad pre-edge features p_1 and p_3 at the Ti K-edge are still unknown, most likely localized and containing d character embedded into the conduction band, the highly intensified pre-edge resonances together with the negative shift of its edge onset as well as main-edge peak compared to TiO_2 and Ti_2O_3 certainly corroborate its metallic Ti^0 character.[7,15]

Figure 4b shows the evolution of the Ti K-edge TEY XANES spectra of amorphous NT specimens upon Na^+ uptake/release. Before the initial discharge, am-1 exhibits an intense peak p_3 as well as two shoulder features p_1 and p_5 at the Ti K pre-edge region, which indicates the distorted or defective Ti local environment with tetrahedral or pentahedral coordination in the amorphous structure.[7,38,39] After being discharged to 0.5 V, am-2 undergoes a dramatic spectral change by showing a

DOI: 10.1021/acs.jpcc.7b01106
J. Phys. Chem. C 2017, 121, 11773−11782

metallic Ti-like XANES pattern with intense peaks p_1 and p_3 together with the negative shift of its main-edge feature. The surface/near surface formation of metallic Ti is further confirmed by the Ti K-edge TEY XANES of am-3. Once amorphous NTs are discharged to 0.01 V, the retention of strong features p_1 and p_3 as well as the further negative shift of main-edge feature of am-3 compared to am-2 evidently suggests that the introduction of Na^+ into the surface/near surface titania lattice not only can induce the reduction of Ti^{4+} into Ti^{3+} for charge neutrality considerations as suggested earlier[15] but also is capable of reducing TiO_2 further into metallic Ti after the electrochemical reaction.

By charging back to 0.9 V, despite the characteristics of metallic Ti at the pre-edge region being retained, am-4 endures a partial oxidization along with the extraction of Na^+ as its main-edge feature at the Ti K-edge exhibits a positive shift compared to am-3. Once the amorphous NTs are fully charged to 2 V, the general Ti K-edge spectrum pattern of am-5 resembles that of am-1, rendering the amorphous TiO_2 NT as a suitable host for the Na^+ accommodation. Nonetheless, the XANES spectrum of am-5 shows the more intense pre-edge features and a slightly negative shift of its edge onset compared to that of am-1, demonstrating that the reduction induced by Na^+ insertion is not fully reversible. It reveals that a small amount of Na^+ inserted into the amorphous TiO_2 lattice from initial discharge would remain in the host structure even after initially full charge rather than have a fully reversible extraction, which echoes the EDX analysis after the first cycle discussed above. Note that in contradiction to the reversible Na^+ insertion/extraction in amorphous TiO_2 reported in previous studies,[15,16] for the first time we show the formation of metallic Ti on the surface/near surface as well as the evidence for irreversible Na^+ uptake/release in amorphous TiO_2 NT matrix, which, however, is similar to the recent study of Na^+ insertion in anatase TiO_2 nanoparticles.[8]

Figure 4c illustrates the evolution of the local structure of surface/near surface Ti at the Ti K-edge of anatase NTs upon Na^+ intercalation/deintercalation. Both c-1 and c-2 share the same anatase TiO_2 XANES profile. It indicates that the electrochemical reaction at the discharging potential range of 2.2−0.5 V mainly results in the electrolyte decomposition and/or the formation of solid electrolyte interphase (SEI)[8,14] rather than the reaction of Na^+ with anatase TiO_2, in accord with the above XRD analysis (Figure 3). As the anatase NTs are discharged to 0.01 V, an abrupt change is observed at the Ti K-edge TEY XANES of c-3: at the pre-edge, the general broad and intense features are displayed, where the metallic Ti characteristics (peaks p_1 and p_3) are now noticeable, suggesting the surface/near surface reduction of Ti^{4+} (TiO_2) into Ti^0 upon its interaction with Na^+ as mentioned above. Meantime, the decrease of Ti oxidation states in c-3 can be further confirmed by the negative shift of its edge onset and the variation of its main-edge feature, where the peak intensity sharply drops as extra electrons fill the Ti 3d orbitals (hybridized with Ti 4p). Furthermore, the flattening of the main-edge features of c-3 compared to the pronounced main-edge fine structures of c-1 and c-2 (crystalline anatase) indicates the sabotage of long-range order of anatase TiO_2 upon Na^+ insertion. Partial oxidation process takes place as the Na^+ extraction proceeds. Hence, both c-4 and c-5 show the decrease of pre-edge features while the increase of main-edge peaks. Nevertheless, once fully charged to 2 V, neither the pre-edge nor the main-edge of c-5 holds the anatase XANES features. Instead, an amorphous-like Ti K-edge spectrum of c-5 analogous to that of am-5 is shown, corroborating the XRD finding (Figure 3) that an irreversible surface/near surface amorphization process takes place in anatase TiO_2 NTs upon Na^+ uptake/release.

Since the X-ray attenuation length at the Ti K-edge (~10 μm, Figure S7) is much larger than the tube length of the as-made TiO_2 NTs (~4 μm, Figure S3), the predominant Ti features from the Ti substrate are mainly observed from the Ti K-edge PFY XANES spectra (not shown). Henceforth, PFY XANES at the Ti $L_{3,2}$-edge (with X-ray probing length of hundreds of nanometers as indicated in Figure S7) is utilized in this study to track the bulk Ti local structure evolution during Na^+ insertion/extraction. Note that TEY XANES at the Ti $L_{3,2}$-edge (with a probing depth of several nanometers) also can deliver the surface local structure of Ti species. Nonetheless, the discharged/charged TiO_2 specimens suffer the oxidation effect, consistent with the previous report;[8] hence only oxidized Ti features are observed from the Ti $L_{3,2}$-edge TEY XANES analysis (Figure S8). Instead, the formation of metallic Ti is resolved by the Ti K-edge TEY XANES (with a probing depth of tens of nanometers) as the TEY detection depth at the K-edge is much larger than that at the L-edge due to the much higher incident photon energy of the former edge.

Figure 4d shows the Ti $L_{3,2}$-edge PFY XANES spectra of Ti foil, Ti_2O_3, anatase and rutile TiO_2 standards. The interpretations of fine structures a−g are well established:[26,30] whereas the two resonances a and b at the pre-edge region can be attributed to core-hole−d-electron interactions, feature c and the doublet (d + e) at the Ti L_3-edge result from electronic transitions from the Ti $2p_{3/2}$ to t_{2g} and e_g states, respectively, and electronic transitions from the Ti $2p_{1/2}$ to t_{2g} and e_g states correspond to the respective origins of peaks f and g at the Ti L_2-edge. Since the Ti e_g orbitals align toward the O 2p orbitals, the Ti L_3-e_g peak (doublet peaks d and e) possesses high sensitivity of the Ti local environment, i.e., local symmetry and oxidation state.[26] For anatase and rutile TiO_2 (Ti^{4+}), the intensity of the dominant peak d over that of e of the former as well as the reverse case for the latter denotes their different local symmetries of D_{2d} and D_{2h}, respectively. As an extra electron fills in the Ti 3d orbital, the Ti $L_{3,2}$-edge XANES of Ti_2O_3 (Ti^{3+}) exhibits a red shift and broadening due to the Jahn−Teller distortion as well as exchange interaction, which is in good agreement with previous reports.[26,27] As for Ti foil with more electrons occupying the Ti 3d orbital, the Ti $L_{3,2}$-edge PFY XANES of Ti metal expectedly delivers a further broad spectrum together with a red shift compared to that of Ti_2O_3. It should be mentioned that the Ti $L_{3,2}$-edge PFY spectra shown here get damped (i.e., less-resolved) due to self-absorption.[26,30]

Figure 4e compiles the Ti $L_{3,2}$-edge PFY XANES of amorphous NT specimens discharged/charged at different potentials. Since the as-grown NTs are amorphous and have the distorted local symmetry and a rich amount of Ti^{3+} states, the Ti $L_{3,2}$-edge spectrum of am-1 shows a general broad pattern without the splitting of peak d.[27] Upon Na^+ uptake/release, the bulk Ti local structure shows no obvious change except the XANES spectrum of am-3 has a better resolvability compared to those of the rest of the four, which unequivocally results from the damping of self-absorption due to the presence of the flower-like structure (containing Na, C, and O as shown in Figure 2) residing on the top of amorphous TiO_2 NTs (Figure 1d). Because the incoming X-ray will reach a shallower depth in this NT specimen than the others due to the interference of the top layer (without Ti) with absorption and scattering, the

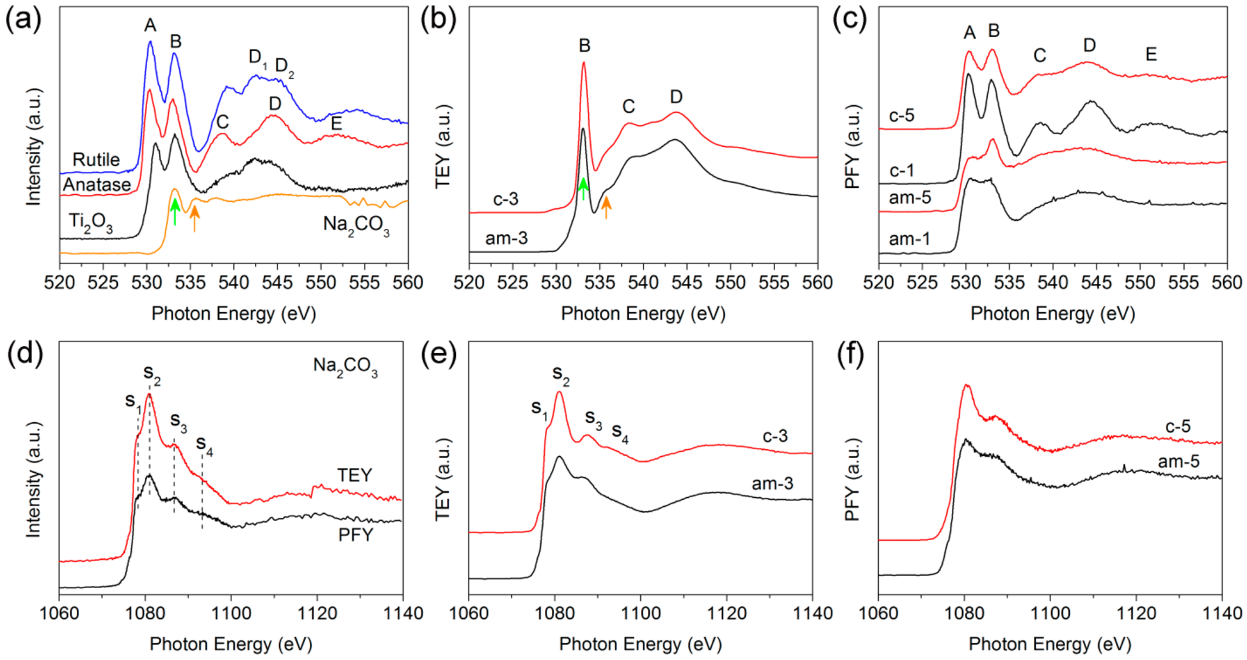

Figure 5. O K-edge XANES spectra of (a) standards including Na_2CO_3, Ti_2O_3, anatase and rutile TiO_2, (b) am-3 and c-3 recorded in TEY mode, and (c) am-1, am-5, c-1, and c-5 recorded in PFY mode. Na K-edge XANES of (d) Na_2CO_3 recorded in both TEY and PFY modes, (e) am-3 and c-3 recorded in TEY mode, and (f) am-5 and c-5 recorded in PFY mode.

outcoming Ti Lα fluorescence X-ray would suffer less self-absorption in am-3, leading to sharper features. More importantly, the barely changed Ti local structure in the bulk of amorphous NT specimens upon Na^+ insertion/extraction indicates that the bulk structure of Ti is well maintained during the discharge/charge process.

A closer observation at the spectral features reveals a broad dip at ~461 eV (highlighted by orange arrow), corresponding to Ti^{3+} character (Figure 4d), for all the discharged and charged specimens (except am-1), confirming a reduction of Ti^{4+} to Ti^{3+} in TiO_2 upon Na^+ intercalation.[9,15] Moreover, the retention of Ti^{3+} feature at ~461 eV at the Ti $L_{3,2}$-edge XANES of am-5 suggests that part of the initially inserted Na^+ would rather stay in the host structure instead of having a reversible extraction, consistent with the residual sodium components detected by EDX (Figure S4). In addition, the metallic Ti signal, clearly resolved by the surface/near surface analysis at the Ti K-edge TEY XANES (Figure 4b), is not shown in the current bulk characterization as no severe broadening or a negative shift of Ti $L_{3,2}$-edge PFY spectrum is observed by comparing to the standards (Figure 4d). It indicates that the reduction of TiO_2 to metallic Ti only occurs on the surface/near surface of amorphous NTs where the initial formation of metastable sodium titanate on the surface/near surface upon Na^+ insertion would be further converted into metallic Ti due to the drastically electrochemical interaction at the electrolyte/electrode interface.[8] Nevertheless, the insertion of Na^+ into the bulk amorphous TiO_2 lattice forms the more stable sodium titanate species.

As for the tracking of the Na^+ uptake/release process in the bulk anatase lattice, Figure 4c provides the Ti $L_{3,2}$-edge PFY XANES of the crystalline anatase NT specimens discharged/charged at different potentials. Within the discharging potential of 1.8−0.5 V, no change of anatase XANES profile is seen between c-1 and c-2, agreeing with the results revealed at the Ti K-edge (Figure 4c). As the potential drops to 0.01 V, the anatase characteristics disappear; instead, c-3 shows a Ti $L_{3,2}$-edge XANES pattern resembling an amorphous structure. Interestingly, it is analogous to the Ti $L_{3,2}$-edge PFY XANES of am-3 where the enhanced spectral resolvability due to the reduction of self-absorption mentioned above is clearly shown. As the Na^+ extraction proceeds along with the charging process, both c-4 and c-5 display very similar amorphous Ti $L_{3,2}$-edge PFY XANES profiles, indicating that the irreversible anatase to amorphous transformation upon Na^+ insertion not only occurs on the surface/near surface of initial crystalline TiO_2 (Figure 4c) but also happens to the bulk of anatase TiO_2 lattice. Nonetheless, the formation of bulk sodium titanate is comparatively stable such that no metallic Ti signal is detected, in contrast to the surface/near surface analysis.

Therefore, the above surface/near surface and bulk analyses from the Ti perspectives manifest great significance. At first, by discharge to 0.5 V, the insertion of Na^+ takes place in amorphous TiO_2 NT but not in anatase one, indicating that the sodiation reaction in the former requires less energy than that in the latter. It can be attributed to the more active nature of amorphous TiO_2 which holds a highly distorted and porous structure with rich defects on its surface for the easier adsorption and reaction of Na^+,[27] corroborating the much greater areal capacity achieved in amorphous TiO_2 NTs within the discharging potential range of 2.2−0.5 V (Figure 1a). Meantime, the electrochemical reaction between Na^+ and amorphous TiO_2 results in the formation of metastable and stable sodium titanates on the surface/near surface and the in the bulk, respectively, of which the former would be further reduced to metallic Ti along with the Na^+ interaction. Then by a further discharging to 0.01 V, the Na^+ intercalation proceeds further in amorphous NTs but it is first initiated in anatase NTs, suggesting that sodiation of anatase TiO_2 starts at a lower voltage than amorphous one. It totally explains why Xiong et al.[15] only observed the electrochemical activity of amorphous TiO_2 but not the anatase one in their SIB performance by using a cutoff discharge potential of 0.5 V. At this point, the portion of metallic Ti of c-3 revealed by the Ti K-edge analysis is not as significant as that of am-3. It indicates that amorphous TiO_2 can uptake more Na^+ than its anatase counterpart at the same potential, which is in agreement with its higher total areal capacity at 0.01 V (Figure 1a). Nevertheless, anatase TiO_2 with its two-dimensional Na^+ diffusion tunnels (Figure S1) shows its fast Na^+ uptake capability after its initialization at a lower discharge potential, which achieves a greater areal capacity within the potential range of 0.5−0.01 V than amorphous NTs as a comparison demonstrated in Figure 1a and Figure 1b. Moreover, both amorphous and anatase host structures exhibit the similar amorphous structures at the fully discharged state, analogous to the amorphous sodium titanate.[40]

The above-described observation delivers a clear message that whatever the initial host structure is (i.e., amorphous or anatase), the electrochemical reaction of TiO_2 with Na^+ would inevitably result in the amorphization of host structures. Particularly for crystalline anatase TiO_2, the large stress and strain induced by the accommodation of large Na^+ would distort both the local structure of TiO_6 and its long-range connectivity. Lastly, it appears noteworthy that this amorphization transition is irreversible as shown in Figures 3 and 4.

Na^+ Insertion and Extraction: O and Na Perspectives. We now return to the flower-like structures (containing Na, C, and O as shown in Figure 2) that appear in the discharge process and disappear in the charge process along with the Na^+ uptake/release as well as the formation/disappearance of metallic Ti during the first cycle. It is highly necessary to provide structural analysis of those structures to further understand the Na^+ interaction with TiO_2 NTs. Moreover, the irreversible amorphization phenomenon during the Na^+ insertion/extraction is discovered based on the above Ti local structure analysis; hence, it is essential to scrutinize the electronic structures of the fully charged materials (i.e., sodium titanate), which allow for the reversible Na^+ uptake/release in the following cycling and are responsible for the superior cyclability (Figure S2). Therefore, XANES analysis from the O (Figure 5a−c) and Na (Figure 5d−f) perspectives has been carried out.

First, as flower-like structures cover most of the electrode surface by discharging at 0.01 V (Figure 1d and Figure 1g), their structural analysis is accomplished by inspecting the surfaces of am-3 and c-3 using TEY XANES. Figure 5a shows the O K-edge XANES of standard Na_2CO_3, Ti_2O_3, anatase and rutile TiO_2 for comparison. In general, except Na_2CO_3, the O K-edge XANES more or less shows the typical TiO_2 features A−E. Whereas the origins of peaks A and B can be assigned to the electronic transitions from O 1s to 2p covalently hybridized with the t_{2g} and e_g states of Ti 3d, respectively, peaks C and D result from the O 2p hybridized with the Ti 4s and 4p states, and the presence of feature E usually suggests the long-range order of the associated structure.[26,27,30] By comparison with standards, the O K-edge TEY XANES spectra of both am-3 and c-3 (Figure 5b) exhibit the dominant Na_2CO_3 features (indicated by green and orange arrows) coupled with TiO_2 features (peaks C, D, and possibly B), which clearly illustrate that the flower-like structures covered on the top of electrodes are mainly Na_2CO_3. Further evidence is provided by the Na K-edge XANES analysis. In general, Na K-edge absorption involves the electronic transition from Na 1s to 3p states, which brings the four distinct resonances (s_1−s_4) at the main-edge region of Na_2CO_3 (Figure 5d).[40] Consistently, the Na K-edge TEY XANES spectra of both am-3 and c-3 deliver the characteristic Na_2CO_3 features, which doubly confirm the Na_2CO_3 nature of these flower-like structures. Nonetheless, results from a recent report point out that the similar flower-like structures hold a pseudo-amorphous form with a chemical structure close to NaO_2,[8] in contrast to our Na_2CO_3 finding revealed by EDX mapping (Figure 2) and the O K-edge and Na K-edge analysis (Figure 5b and Figure 5e). We believe that since the claimed NaO_2 in the literature is extremely unstable, so we conjecture that the formation of Na_2CO_3 is a more common form in SIB material study using a carbonate-based electrolyte.[40]

Second, in order to investigate the electronic structures of fully charged amorphous and anatase TiO_2 NTs with respect to their differences compared to those fresh ones before discharging, XANES spectra recorded in PFY mode are collected at the O K-edge and Na K-edge. Note that PFY rather than TEY XANES mode is applied to distinguish the O and Na local structures of fully charged NTs from those of surface Na_2CO_3 residuals.

As shown in Figure 5c, by comparison of the O K-edge PFY XANES of am-1 and am-5, a general broad spectral pattern together with the enhanced intensity of peak B in am-5 is observed. Similar change also happens to the anatase NTs before discharging (c-1) and after fully charging (c-5), albeit the intensity increase of peak B in c-5 is not as significant as that in am-5. A couple of features must be noted. First, the broadening of O K-edge XANES indicates the O local structures in both amorphous and anatase NTs are distorted after the first cycle of Na^+ insertion/extraction.[26] In particular, the anatase host structure suffers the breakage of its long-range order as features C, D, and E are smoothed out noticeably. Second, the enhanced intensity of peak B could be due to the contribution of (1) Na_2CO_3 impurity (resonance at the energy location of feature B in Figure 5a) or (2) reduced Ti oxide species (e.g., Ti_2O_3 exhibits intense peak B over A in Figure 5a) or (3) the change of O−Ti coordination number and the connectivity of the TiO_6 aroused by the leftover Na^+ in NTs after fully charging.[40] To confirm the third point, Figure 5f includes the Na K-edge PFY XANES of am-5 and c-5. Unlike the several resonances s_1−s_4 shown at the Na K-edge XANES of Na_2CO_3 (Figure 5d), both am-5 and c-5 exhibit the two similar broad features located between 1080 and 1100 eV, which are in accordance with our previous report of amorphous sodium titanate,[40] where the form of broad features typically indicates the local order of Na^+.[40−42] Therefore, results from both O and Na perspectives are in alignment with the above Ti analysis and unambiguously reveal that both amorphous and anatase TiO_2 NTs transform to the amorphous sodium titanate NTs after the first cycle of Na^+ insertion/extraction. It is worth noting that the sodiated titanates result from two different host materials and because of their history might exhibit different electronic behavior, which totally explains why they provide different areal capacities for the long-term cyclability although both of them deliver the reversible Na^+ uptake/release capability (Figure S2).

■ CONCLUSIONS

Highly ordered TiO_2 NT arrays in both amorphous and anatase phases have been synthesized using electrochemical anodization, coupled with a postannealing process for the preparation of the latter. The electrochemical interaction between Na^+ and TiO_2 has been investigated using these amorphous and anatase TiO_2 NTs as anode materials for the cycling of Na^+ uptake/

release. The associated local structure variations of amorphous and anatase TiO_2 at the first cycle are comparatively examined using XANES. From the electrochemical perspective, amorphous TiO_2 NTs exhibit a lower sodiation potential and higher areal capacity than anatase ones due to the distorted structure, porosity, and rich defects involved in the former, allowing easier accommodation of Na^+ than the latter. Nonetheless, anatase TiO_2 with its two-dimensional ionic diffusion tunnels can also uptake Na^+ quickly after initial sodiation. From the XANES results, we find that the surfaces/near surfaces of amorphous and anatase TiO_2 NTs show a partial reduction of TiO_2 into metallic Ti upon initial Na^+ insertion, which is most likely due to the decomposition of unstable sodium titanate formed at the electrolyte/electrode interface. Meantime, amorphous TiO_2 NT with its more active nature results in a larger amount of metallic Ti than its anatase counterpart during initial sodiation. More interestingly, the surface/near surface XANES analysis reveals that both amorphous and anatase TiO_2 NTs undergo irreversible phase transformations to amorphous sodium titanates after full charge at the first cycle; similar irreversible process with the formation of stable amorphous sodium titanate in the bulk is also found from the bulk sensitive XANES characterization. Accordingly, these newly formed structures, other than the original amorphous and anatase TiO_2, are responsible for the subsequent battery performance. Further analysis is underway to characterize the as-formed amorphous sodium titanates, where a detailed structural analysis will contribute to the understanding of the process and hence a pathway leading to the optimal performance of these materials for functional battery design.

■ ASSOCIATED CONTENT

Ⓢ Supporting Information

The Supporting Information is available free of charge on the ACS Publications website at DOI: 10.1021/acs.jpcc.7b01106.

> Crystal structure projections, electrochemical cycling data, SEM, EDX, and XRD results, calculated X-ray attenuation length, and the Ti $L_{3,2}$-edge TEY XANES (PDF)

■ AUTHOR INFORMATION

Corresponding Authors

*X. Sun: e-mail, xsun9@uwo.ca.

*T.-K. Sham: e-mail, tsham@uwo.ca.

ORCID

Jun Li: 0000-0002-1958-5665

Xueliang Sun: 0000-0003-2881-8237

Present Address

⊥School of Engineering, Faculty of Applied Science, University of British Columbia, Kelowna, British Columbia V1V 1V7, Canada.

Author Contributions

‖J. Li and J. Liu contributed equally to this work

Notes

The authors declare no competing financial interest.

■ ACKNOWLEDGMENTS

Research at the University of Western Ontario is supported by the Discovery grant of the Natural Science and Engineering Research Council of Canada (NSERC), the Canada Research Chair (CRC) Program, the Canada Foundation for Innovation (CFI), and the Interdisciplinary Initiative (IDI) grant of the University of Western Ontario (UWO). The work at the Canadian Light Source (CLS) is supported by CFI, NSERC, the University of Saskatchewan, the Government of Saskatchewan, Western Economic Diversification Canada, the National Research Council Canada, and the Canadian Institute for Health Research (CIHR). We thank Dr. T. Regier, Dr. Q. F. Xiao, and Dr. Y. F. Hu for their technical support at the SGM and SXRMB beamlines at CLS. Dr. J. Li acknowledges the receipt of support from the CLS Graduate Student Travel Support Program. Dr. J. Liu is really grateful for the financial support from NSERC Postdoctoral Fellowship (PDF) Program.

■ REFERENCES

(1) Ye, M. D.; Gong, J. J.; Lai, Y. K.; Lin, C. J.; Lin, Z. Q. High-Efficiency Photoelectrocatalytic Hydrogen Generation Enabled by Palladium Quantum Dots-Sensitized TiO_2 Nanotube Arrays. *J. Am. Chem. Soc.* **2012**, *134*, 15720−15723.

(2) Chen, X. B.; Liu, L.; Yu, P. Y.; Mao, S. S. Increasing Solar Absorption for Photocatalysis with Black Hydrogenated Titanium Dioxide Nanocrystals. *Science* **2011**, *331*, 746−750.

(3) Zhu, K.; Neale, N. R.; Miedaner, A.; Frank, A. J. Enhanced Charge-Collection Efficiencies and Light Scattering in Dye-Sensitized Solar Cells Using Oriented TiO_2 Nanotubes Arrays. *Nano Lett.* **2007**, *7*, 69−74.

(4) Crossland, E. J. W.; Noel, N.; Sivaram, V.; Leijtens, T.; Alexander-Webber, J. A.; Snaith, H. J. Mesoporous TiO_2 Single Crystals Delivering Enhanced Mobility and Optoelectronic Device Performance. *Nature* **2013**, *495*, 215−219.

(5) Lu, X. H.; Wang, G. M.; Zhai, T.; Yu, M. H.; Gan, J. Y.; Tong, Y. X.; Li, Y. Hydrogenated TiO_2 Nanotube Arrays for Supercapacitors. *Nano Lett.* **2012**, *12*, 1690−1696.

(6) Kim, H.; Cho, M. Y.; Kim, M. H.; Park, K. Y.; Gwon, H.; Lee, Y.; Roh, K. C.; Kang, K. A Novel High-Energy Hybrid Supercapacitor with An Anatase TiO_2-Reduced Graphene Oxide Anode and An Activated Carbon Cathode. *Adv. Energy Mater.* **2013**, *3*, 1500−1506.

(7) Wang, D. N.; Liu, L. J.; Sun, X. L.; Sham, T. K. Observation of Lithiation-Induced Structural Variations in TiO_2 Nanotube Arrays by X-ray Absorption Fine Structure. *J. Mater. Chem. A* **2015**, *3*, 412−419.

(8) Wu, L. M.; Bresser, D.; Buchholz, D.; Giffin, G. A.; Castro, C. R.; Ochel, A.; Passerini, S. Unfolding the Mechanism of Sodium Insertion in Anatase TiO_2 Nanoparticles. *Adv. Energy Mater.* **2015**, *5*, 1401142.

(9) Kim, K. T.; Ali, G.; Chung, K. Y.; Yoon, C. S.; Yashiro, H.; Sun, Y. K.; Lu, J.; Amine, K.; Myung, S. T. Anatase Titania Nanorods as An Intercalation Anode Material for Rechargeable Sodium Batteries. *Nano Lett.* **2014**, *14*, 416−422.

(10) Fang, H. T.; Liu, M.; Wang, D. W.; Sun, T.; Guan, D. S.; Li, F.; Zhou, J. G.; Sham, T. K.; Cheng, H. M. Comparison of the Rate Capability of Nanostructured Amorphous and Anatase TiO_2 for Lithium Insertion Using Anodic TiO_2 Nanotube Arrays. *Nanotechnology* **2009**, *20*, 225701.

(11) Lunell, S.; Stashans, A.; Ojamae, L.; Lindstrom, H.; Hagfeldt, A. Li and Na Diffusion in TiO_2 from Quantum Chemical Theory Versus Electrochemical Experiment. *J. Am. Chem. Soc.* **1997**, *119*, 7374−7380.

(12) Bresser, D.; Paillard, E.; Binetti, E.; Krueger, S.; Striccoli, M.; Winter, M.; Passerini, S. Percolating Networks of TiO_2 Nanorods and Carbon for High Power Lithium Insertion Electrodes. *J. Power Sources* **2012**, *206*, 301−309.

(13) Wagemaker, M.; Borghols, W. J. H.; Mulder, F. M. Large Impact of Particle Size on Insertion Reactions. A Case for Anatase Li_xTiO_2. *J. Am. Chem. Soc.* **2007**, *129*, 4323−4327.

(14) Gonzalez, J. R.; Alcantara, R.; Nacimiento, F.; Ortiz, G. F.; Tirado, J. L. Microstructure of the Epitaxial Film of Anatase Nanotubes Obtained at High Voltage and the Mechanism of Its Electrochemical Reaction with Sodium. *CrystEngComm* **2014**, *16*, 4602−4609.

(15) Xiong, H.; Slater, M. D.; Balasubramanian, M.; Johnson, C. S.; Rajh, T. Amorphous TiO_2 Nanotube Anode for Rechargeable Sodium Ion Batteries. *J. Phys. Chem. Lett.* **2011**, *2*, 2560−2565.

(16) Gonzalez, J. R.; Alcantara, R.; Ortiz, G. F.; Nacimiento, F.; Tirado, J. L. Controlled Growth and Application in Lithium and Sodium Batteries of High-Aspect-Ratio, Self-Organized Titania Nanotubes. *J. Electrochem. Soc.* **2013**, *160*, A1390−A1398.

(17) Yang, X. M.; Wang, C.; Yang, Y. C.; Zhang, Y.; Jia, X. N.; Chen, J.; Ji, X. B. Anatase TiO_2 Nanocubes for Fast and Durable Sodium Ion Battery Anodes. *J. Mater. Chem. A* **2015**, *3*, 8800−8807.

(18) Xu, Y.; Lotfabad, E. M.; Wang, H. L.; Farbod, B.; Xu, Z. W.; Kohandehghan, A.; Mitlin, D. Nanocrystalline Anatase TiO_2: A New Anode Material for Rechargeable Sodium Ion Batteries. *Chem. Commun.* **2013**, *49*, 8973−8975.

(19) Su, D. W.; Dou, S. X.; Wang, G. X. Anatase TiO_2: Better Anode Material Than Amorphous and Rutile Phases of TiO_2 for Na-Ion Batteries. *Chem. Mater.* **2015**, *27*, 6022−6029.

(20) Wu, L. M.; Buchholz, D.; Bresser, D.; Chagas, L. G.; Passerini, S. Anatase TiO_2 Nanoparticles for High Power Sodium-Ion Anodes. *J. Power Sources* **2014**, *251*, 379−385.

(21) Ni, J. F.; Fu, S. D.; Wu, C.; Maier, J.; Yu, Y.; Li, L. Self-Supported Nanotube Arrays of Sulfur-Doped TiO_2 Enabling Ultrastable and Robust Sodium Storage. *Adv. Mater.* **2016**, *28*, 2259−2265.

(22) Das, S. K.; Jache, B.; Lahon, H.; Bender, C. L.; Janek, J.; Adelhelm, P. Graphene Mediated Improved Sodium Storage in Nanocrystalline Anatase TiO_2 for Sodium Ion Batteries with Ether Electrolyte. *Chem. Commun.* **2016**, *52*, 1428−1431.

(23) Tahir, M. N.; Oschmann, B.; Buchholz, D.; Dou, X. W.; Lieberwirth, I.; Panthofer, M.; Tremel, W.; Zentel, R.; Passerini, S. Extraordinary Performance of Carbon-Coated Anatase TiO_2 as Sodium-Ion Anode. *Adv. Energy Mater.* **2016**, *6*, 1501489.

(24) Cha, H. A.; Jeong, H. M.; Kang, J. K. Nitrogen-Doped Open Pore Channeled Graphene Facilitating Electrochemical Performance of TiO_2 Nanoparticles as An Anode Material for Sodium Ion Batteries. *J. Mater. Chem. A* **2014**, *2*, 5182−5186.

(25) Hwang, J. Y.; Myung, S. T.; Lee, J. H.; Abouimrane, A.; Belharouak, I.; Sun, Y. K. Ultrafast Sodium Storage in Anatase TiO_2 Nanoparticles Embedded on Carbon Nanotubes. *Nano Energy* **2015**, *16*, 218−226.

(26) Li, J.; Liu, C. H.; Li, X.; Wang, Z. Q.; Shao, Y. C.; Wang, S. D.; Sun, X. L.; Pong, W. F.; Guo, J. H.; Sham, T. K. Unraveling the Origin of Visible Light Capture by Core-Shell TiO_2 Nanotubes. *Chem. Mater.* **2016**, *28*, 4467−4475.

(27) Li, J.; Liu, C. H.; Ye, Y. F.; Zhu, J. F.; Wang, S. D.; Guo, J. H.; Sham, T. K. Tracking the Local Effect of Fluorine Self-Doping in Anodic TiO_2 Nanotubes. *J. Phys. Chem. C* **2016**, *120*, 4623−4628.

(28) Hu, Y. F.; Coulthard, I.; Chevrier, D.; Wright, G.; Igarashi, R.; Sitnikov, A.; Yates, B. W.; Hallin, E. L.; Sham, T. K.; Reininger, R. Preliminary Commissioning and Performance of the Soft X-ray Micro-Characterization Beamline at the Canadian Light Source. *AIP Conf. Proc.* **2009**, *1234*, 343−346.

(29) Regier, T.; Paulsen, J.; Wright, G.; Coulthard, I.; Tan, K.; Sham, T. K.; Blyth, R. I. R. In Commissioning of the Spherical Grating Monochromator Soft X-ray Spectroscopy Beamline at the Canadian Light Source. *AIP Conf. Proc.* **2006**, *879*, 473−476.

(30) Li, J.; Liu, L. J.; Sham, T. K. 2D XANES-XEOL Spectroscopy Studies of Morphology-Dependent Phase Transformation and Corresponding Luminescence from Hierarchical TiO_2 Nanostructures. *Chem. Mater.* **2015**, *27*, 3021−3029.

(31) Farges, F.; Brown, G. E.; Rehr, J. J. Ti K-Edge XANES Studies of Ti Coordination and Disorder in Oxide Compounds: Comparison between Theory and Experiment. *Phys. Rev. B: Condens. Matter Mater. Phys.* **1997**, *56*, 1809−1819.

(32) Luca, V.; Djajanti, S.; Howe, R. F. Structural and Electronic Properties of Sol-Gel Titanium Oxides Studied by X-ray Absorption Spectroscopy. *J. Phys. Chem. B* **1998**, *102*, 10650−10657.

(33) Rajh, T.; Nedeljkovic, J. M.; Chen, L. X.; Poluektov, O.; Thurnauer, M. C. Improving Optical and Charge Separation Properties of Nanocrystalline TiO_2 by Surface Modification with Vitamin C. *J. Phys. Chem. B* **1999**, *103*, 3515−3519.

(34) Joly, Y.; Cabaret, D.; Renevier, H.; Natoli, C. R. Electron Population Analysis by Full-Potential X-ray Absorption Simulations. *Phys. Rev. Lett.* **1999**, *82*, 2398−2401.

(35) Wu, Z. Y.; Ouvrard, G.; Gressier, P.; Natoli, C. R. Ti and O K Edges for Titanium Oxides by Multiple Scattering Calculations: Comparison to XAS and EELS Spectra. *Phys. Rev. B: Condens. Matter Mater. Phys.* **1997**, *55*, 10382−10391.

(36) Khan, M. A.; Kotani, A.; Parlebas, J. C. Electronic-Structure and Core Level Photoemission Spectra in TiO_2 Compounds. *J. Phys.: Condens. Matter* **1991**, *3*, 1763−1772.

(37) Okada, K.; Kotani, A. Theory of Core-Level X-ray Photoemission and Photoabsorption in Ti Compounds. *J. Electron Spectrosc. Relat. Phenom.* **1993**, *62*, 131−140.

(38) Stewart, S. J.; Fernandez-Garcia, M.; Belver, C.; Mun, B. S.; Requejo, F. G. Influence of N-Doping on the Structure and Electronic Properties of Titania Nanoparticle Photocatalysts. *J. Phys. Chem. B* **2006**, *110*, 16482−16486.

(39) Chen, L. X.; Rajh, T.; Wang, Z. Y.; Thurnauer, M. C. XAFS Studies of Surface Structures of TiO_2 Nanoparticles and Photocatalytic Reduction of Metal Ions. *J. Phys. Chem. B* **1997**, *101*, 10688−10697.

(40) Liu, J.; Banis, M. N.; Xiao, B. W.; Sun, Q.; Lushington, A.; Li, R. Y.; Guo, J. H.; Sham, T. K.; Sun, X. L. Atomically Precise Growth of Sodium Titanates as Anode Materials for High-Rate and Ultralong Cycle-Life Sodium-Ion Batteries. *J. Mater. Chem. A* **2015**, *3*, 24281−24288.

(41) Cormier, L.; Neuville, D. R. Ca and Na Environments in Na_2O-CaO-Al_2O_3-SiO_2 Glasses: Influence of Cation Mixing and Cation-Network Interactions. *Chem. Geol.* **2004**, *213*, 103−113.

(42) De Wispelaere, S.; Cabaret, D.; Levelut, C.; Rossano, S.; Flank, A. M.; Parent, P.; Farges, F. Na-, Al-, and Si K-Edge XANES Study of Sodium Silicate and Sodium Aluminosilicate Glasses: Influence of the Glass Surface. *Chem. Geol.* **2004**, *213*, 63−70.

DOI: 10.1021/acs.jpcc.7b01106
J. Phys. Chem. C 2017, 121, 11773−11782